Monthly Notices
of the
ROYAL ASTRONOMICAL SOCIETY

Mon. Not. R. Astron. Soc. **406,** 2701–2712 (2010) doi:10.1111/j.1365-2966.2010.16868.x

PG 0907+123 and JL 194: slowly pulsating hot subdwarf stars

C. Koen[1]★ and E. M. Green[2]

[1]*Department of Statistics, University of the Western Cape, Private Bag X17, Bellville, 7535 Cape, South Africa*
[2]*Steward Observatory, University of Arizona, Tucson, AZ 85721, USA*

Accepted 2010 April 19. Received 2010 April 16; in original form 2010 March 12

ABSTRACT

Multicolour time-series photometry of two newly discovered slowly pulsating sdB stars (V1093 Her stars, also known as PG 1716 stars) is described. Both stars are fairly bright and appear, from the limited amount of data, to have rich pulsation spectra. Given that the amplitudes of variation of both stars are also large compared to most PG 1716 stars, both are good candidates for extensive follow-up observations.

Key words: stars: individual: PG 0907+123 – stars: individual: JL 194 – stars: oscillations – subdwarfs – stars: variables: general.

1 INTRODUCTION

The B-type subdwarf (sdB) stars are extended blue horizontal branch (EBHB) stars, between the main sequence and the white dwarfs in the Hertzsprung–Russell diagram. They are evolved, and burn helium in their cores; envelopes, typically hydrogen rich, are too thin to sustain nuclear reactions. Most, if not all, appear to have masses close to $0.5\,M_{\odot}$. Their exact evolutionary paths are a matter of some debate, but substantial mass-loss undoubtedly played a major role in delivering them to the EBHB. A wealth of detail, and a description of the historical development of the study of these stars, can be found in the extensive review by Heber (2009).

Asteroseismology is an avenue for studying the interiors of these stars indirectly, and in the process hopefully gaining a better understanding of their evolution (Østensen 2009). Rapid pulsations (periods typically a few minutes) have been discovered in some of the hotter sdB stars ($T_{\rm eff} > 30\,000$ K). These stars are referred to as EC 14026 (or V361 Hya) stars, after the prototype (Kilkenny et al. 1997). Slower pulsations (periods of 1–2 h) occur in some of the cooler stars (PG 1716 or V1093 Her star – Green et al. 2003a). Three stars near the temperature boundary pulsate on both time-scales (Baran et al. 2005; Schuh et al. 2006; Lutz et al. 2009). Details of only a handful of slowly pulsating sdB stars have been published (see Section 5 for a full list). In this paper we present the discovery of a further two examples.

The star PG 0907+123 was identified as a B-type subdwarf in the Palomar–Green survey (Green, Schmidt & Liebert 1986). The classification was confirmed by Moehler et al. (1990a), who also obtained Strömgren photometry of the star; later photometry by Wesemael et al. (1992) is in reasonable agreement. Moehler, Heber & de Boer (1990b) used the photometry of Moehler et al. (1990a) to derive an effective temperature of 26 300 K, and estimated $\log g = 5.0$ from absorption-line profiles. They also derived a helium abundance of 0.14 per cent, and a distance of 1520 ± 570 pc. Saffer (reported in Billères et al. 2002) found a somewhat higher temperature (27 280 K) and gravity ($\log g = 5.5$), while Maxted et al. (2001) estimated $T_{\rm eff} = 26\,200$ K and $\log g = 5.3$.

It is worth remarking that the temperature and gravity determinations referred to above were based on different assumptions: Moehler et al. (1990a) and Maxted et al. (2001) used solar metallicity line blanketed local thermodynamic equilibrium (LTE) atmospheric models, while Saffer assumed zero metallicity and LTE. A further set of model results is $T_{\rm eff} = 28\,100$ K and $\log g = 5.36$, from zero-metallicity non-LTE (NLTE) models (Fontaine, private communication).

It has been established, from radial velocity measurements, that PG 0907+123 is a binary, with a period of 6.1163 d (Morales-Rueda et al. 2003). Assuming that the mass of the sdB star is $0.5\,M_{\odot}$, the companion has a minimum mass of $0.52\,M_{\odot}$. Interestingly, an earlier study based only on spectral properties found no signs of a companion (Jeffery & Pollacco 1998), and the Two Micron All Sky Survey (2MASS) ($J - H$) value of -0.19 (Skrutskie et al. 2006) is far too blue to accommodate a main-sequence companion with a mass exceeding $0.4\,M_{\odot}$ (e.g. Reed & Stiening 2004).

We have acquired 11 additional radial velocity determinations, spread over several years and bracketing in time the measurements reported by Morales-Rueda et al. (2003) – see Table 1. Our velocities were derived from spectra taken with the MMT Blue spectrograph, always using the identical spectroscopic set-up. The 832 mm^{-1} grating and 1-arcsec slit resulted in a resolution of $R = 4300$ over the wavelength region 4000–4950 Å. The 1996–1997 spectra were obtained with the original MMT configuration of six 1.8-m mirrors; the remaining two spectra were taken after the MMT conversion to a single 6.5-m mirror. Note that the velocity solution combining these velocities with those published by Morales-Rueda et al. (2003) required a constant shift of 7.61 km s^{-1} to be added to the latter velocities. Combining all known radial velocity observations gives an orbital period of 6.116 40(4) d, with a velocity amplitude of 62.5 ± 1.8 km s^{-1}. Even assuming a primary mass as low

★E-mail: ckoen@uwc.ac.za

Table 1. A log of the new radial velocity measurements.

UT date	$T_{\rm exp}$ (s)	HJD (mid-exposure) (245 0000+)	Radial velocity (km s^{-1})	Error (km s^{-1})
1996 January 14	750	0096.737 8279	13.81	1.32
1996 March 11	1000	0153.700 8655	111.74	1.35
1996 December 17	750	0434.942 5232	104.46	1.64
1996 December 17	750	0434.952 0725	107.22	1.98
1996 December 19	750	0436.919 5836	43.85	1.69
1996 December 19	750	0436.929 2372	48.67	1.98
1997 January 2	800	0450.984 3919	−10.54	1.21
1997 March 3	750	0510.783 7443	18.55	1.31
2002 January 23	550	2297.892 0671	−19.60	0.79
2004 January 1	400	3372.011 3702	89.59	1.04

as 0.48 $M_\odot$, a minimum secondary star mass of 0.55 $M_\odot$ is obtained. This is very close to the theoretical upper limit for such systems – see figs 13 and 14 of Han et al. (2003). An orbital inclination smaller than 90° would imply an even larger companion mass.

JL 194 (2000 coordinates $\alpha = 00{:}31{:}41.7, \delta = -47{:}25{:}20.1$) has a number of aliases: LB 1559, CD-48106 and HIP 2499, amongst others. It is listed as a 'violet' star by Jaidee & Lyngrå (1969) (where it is erroneously referred to as LB 1959). Broad-band *UBV* photometry has been published by Hill & Hill (1966) and Wegner (1980), and Strömgren photometry by Kilkenny & Hill (1975) and Newell & Graham (1976). Its first classification as an sdB star was given by Kilkenny & Hill (1975), based on photometric indices; similarly, Newell & Graham (1976) placed it on the hot side of the blue horizontal branch. The sdB classification was confirmed spectroscopically by Heber et al. (1984), who also determined $T_{\rm eff} = 25\,200(\pm1200)$ K and $\log g = 5.2(\pm0.2)$ (based on a line-blanketed LTE model).

JL 194 is listed as a variable star in the Simbad data base, presumably on the basis of the large scatter in its *Hipparcos* photometry, as highlighted by Adelman (2001).

In this paper we report the discovery of pulsations in PG 0907+123 and JL 194. The temperatures and gravities mentioned above place both stars amongst known slowly pulsating sdB stars or PG 1716 stars (e.g. Green et al. 2003b; Fontaine et al. 2006). It is noteworthy that PG 0907+123 has also been monitored for rapid pulsations (Billères et al. 2002), with null results.

2 THE OBSERVATIONS

Photometric observations were made with the South African Astronomical Observatory (SAAO) CCD camera mounted on the 1.0-m telescope at Sutherland. The camera is equipped with a 1024 × 1024 chip, giving a field of view of about 5 arcmin^2. All observations were pre-binned 2 × 2, resulting in a readout time of about 20 s. Measurements were usually made by cycling continuously through the *B*, *V* and *R* filters, but the *R* filter was not used during the first two nights of observing PG 0907+123. Logs of the observations of both stars are given in Table 2. Photometric reductions were completely standard.

In the case of PG 0907+123, the field of view of the SAAO CCD camera included five bright stars, and two to four of these were selected as local standards, depending on results for a given night and filter. Differential profile-fitted magnitudes were found to exhibit less scatter than aperture-photometry magnitudes, and were therefore preferred. The *V*-band results are plotted in Fig. 1. Measurements for the other two filters are similar in appearance, barring the more pronounced effects of differential extinction in the *B*-band observations.

Table 2. The photometric observing logs: $T_{\rm exp}$ is the exposure time and *N* the minimum number of useful measurements per filter obtained during a given run.

Starting time (HJD 245 0000+)	Filter	$T_{\rm exp}$ (s)	Run length (h)	*N*
PG 0907+123				
4891.2804	*BV*	80, 60	2.9	52
4892.2783	*BV*	60–80, 45–60	6.2	110
4893.2652	*BVR*	80, 60, 60	6.7	88
4894.2654	*BVR*	70–80, 60, 60	6.6	87
4895.2658	*BVR*	70–80, 60, 50	6.2	91
JL 194				
5081.3402	*BVR*	50, 40, 40	7.8	140
5084.3048	*BVR*	50, 40, 40	4.1	55
5085.3090	*BVR*	50, 40, 40	8.5	160
5087.3039	*BVR*	35–50, 25–40, 33–40	8.5	170
5090.3158	*BVR*	35–50, 30–40, 30–40	8.1	149

The measurements in Fig. 1 have been placed roughly on an absolute scale, by using the mean $y = 13.95$ of the Strömgren measurements of Moehler et al. (1990a, $y = 13.937$) and Wesemael et al. (1992, $y = 13.970$). The mean *V* magnitude of PG 0907+123 was fixed at $V = 13.95$ on the first night of observing, and its magnitude offset from a bright comparison star noted. Nightly zero-points thereafter were set by the comparison star. The nightly mean *V* magnitude of PG 0907+123 varied by less than 5 millimagnitudes (mmag) over the five runs.

Aperture photometry was superior to image-profile photometry for JL 194. The field of view of JL 194 included two fairly bright stars, and these were used as local comparisons. The mean magnitude of the two stars was used to set nightly zero-points; the range of the night-to-night variations in the mean magnitude of JL 194 was 5 mmag in *V*. The *V*-band light curves are plotted in Fig. 2: substantial frequency beating can be seen, suggesting two or more closely spaced pulsation frequencies with similar amplitudes. The magnitudes can be placed on an absolute scale by replacing the zero mean value by the average $V = 12.375$ of the published photometry.

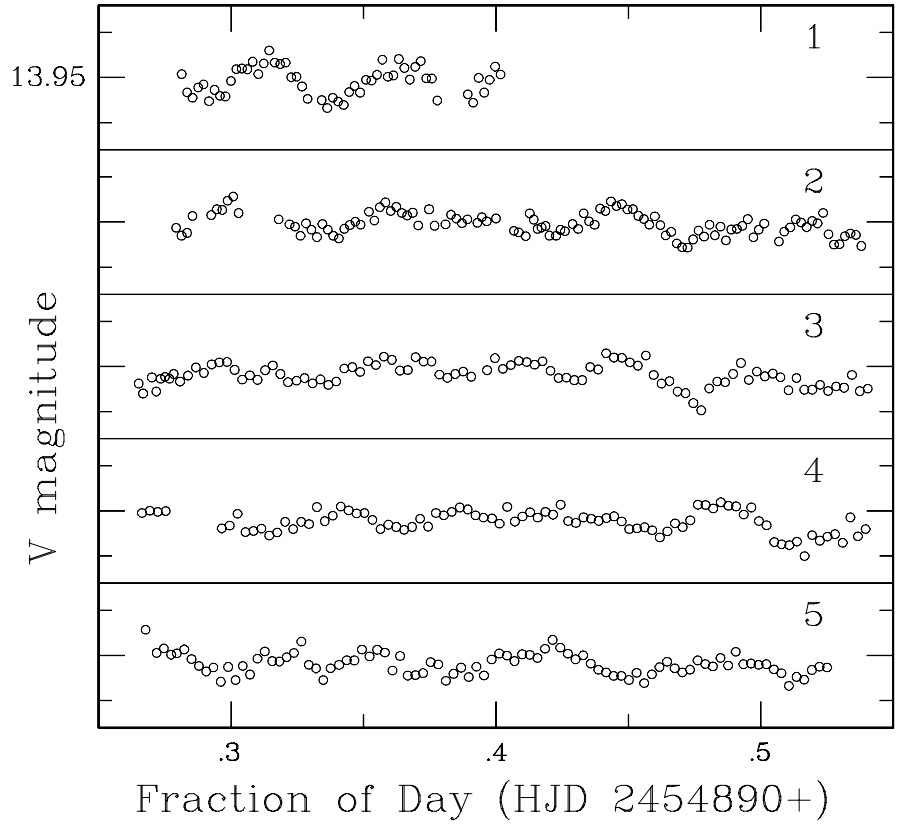

Figure 1. The *V*-band observations of PG 0907+123. Setting of the magnitude zero-points is described in the text. The vertical width of each panel in the plot is 0.08 mag. Panels are labelled with the last digit of the Julian Day of observation.

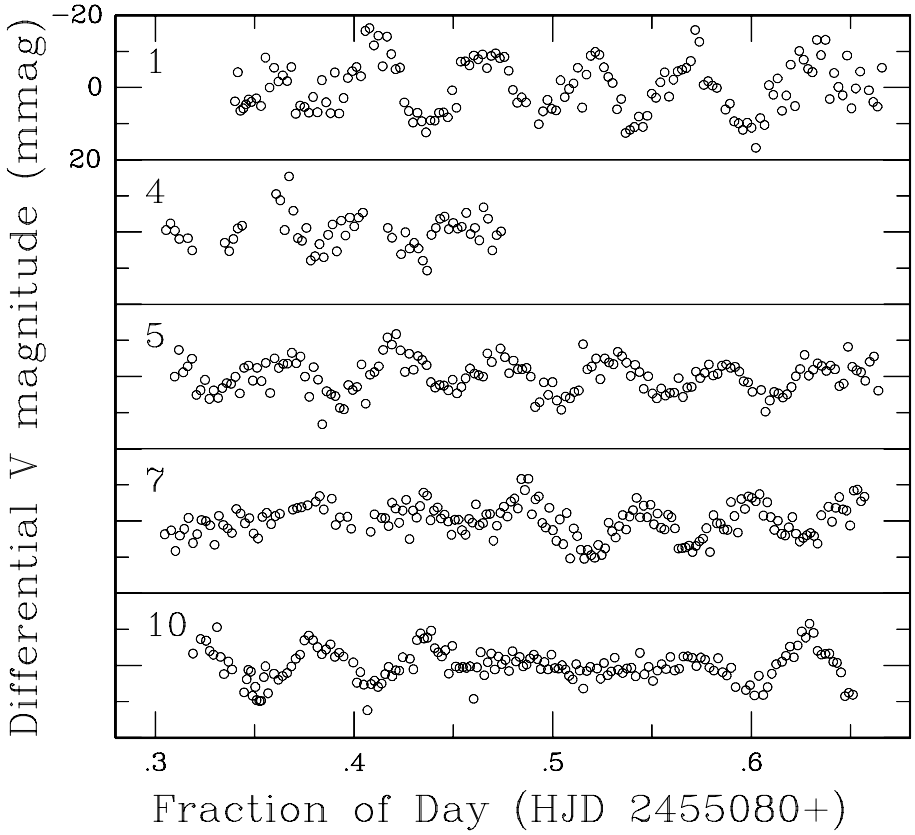

Figure 2. The *V*-band observations of JL 194. The vertical width of each panel in the plot is 0.04 mag. Each run has been detrended by subtraction of a quadratic fit. Panels are labelled with the last digit(s) of the Julian Day of observation.

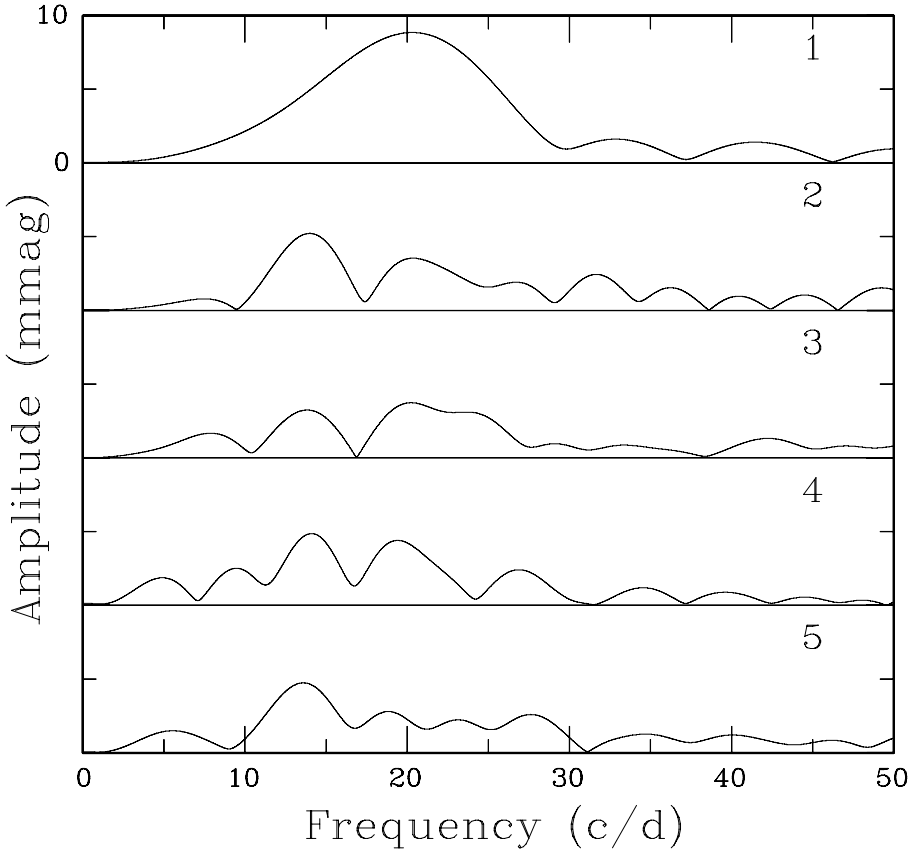

Figure 3. Amplitude spectra of the *V*-band data for PG 0907+123 in Fig. 1. Each night's data were high pass filtered by subtracting a second-order polynomial fit. Panels are labelled with the last digit of the Julian Day of observation.

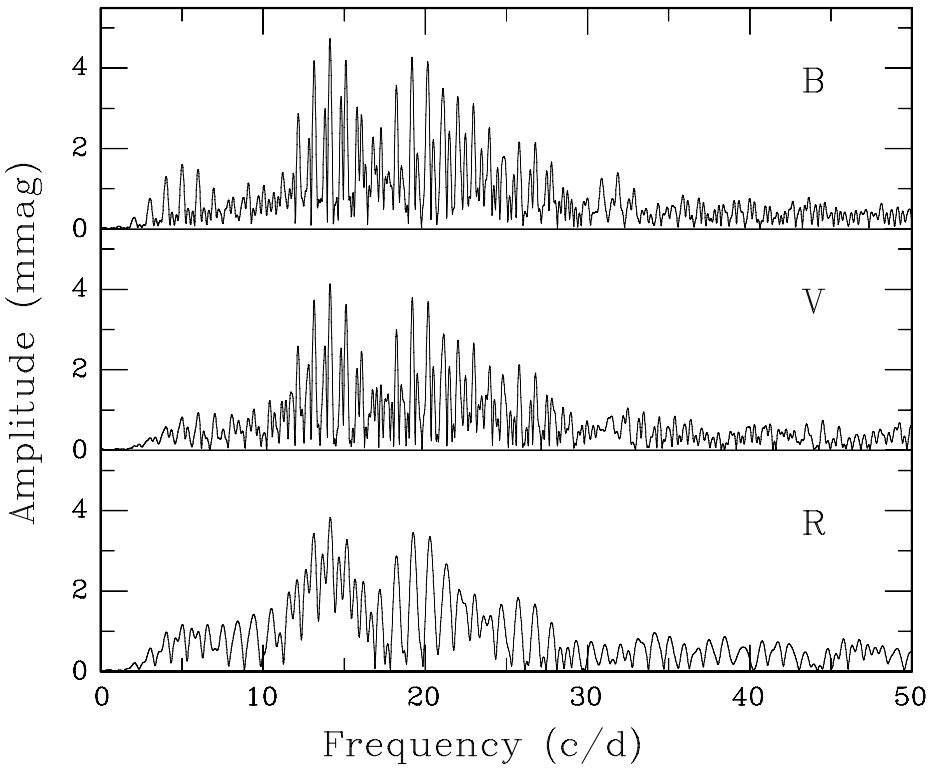

Figure 4. Amplitude spectra of the complete PG 0907+123 data, *B* (top), *V* (middle) and *R* (bottom). Nightly data sets were pre-whitened by subtraction of a least-squares-fitted second-order polynomial.

3 DATA ANALYSIS: PG 0907+123

Amplitude spectra of the data for individual nights shown in Fig. 1 are plotted in Fig. 3. Each nightly data set has been detrended by subtraction of a least-squares-fitted second-order polynomial, in order to remove the effects of differential extinction (since the programme star is expected to be much bluer than the comparison stars). It is clear that the star is multiperiodic, with several frequencies in the range 14–28 d^{-1}. It is also evident that reliable frequencies cannot be extracted from a single night's data.

Amplitude spectra of the full data sets for each of the three filters are given in Fig. 4. Each night's data have again been detrended by subtracting a second-order polynomial. Inspection shows that there are three frequency intervals of excess power, near 14, 20 and 27 d^{-1}. The amplitudes decrease slightly with increasing wavelength, as expected for a PG 1716 star.

There are also conspicuous features near 5 d^{-1} in the *B*-band amplitude spectrum, which are probably due to imperfectly removed differential extinction effects since there is no similar power excess in the *V* or *R* spectra. The highest peak in the spectrum is at 5.02 d^{-1}; this frequency was pre-whitened from the *B*-filter data before proceeding.

The first step in identifying the periodicities in the data is successive pre-whitening of each of the three data sets. The frequency corresponding to the largest peak in the amplitude spectrum is identified, and a sinusoid with this frequency is fitted to the data (i.e. the best-fitting amplitude and phase are determined). The fitted sinusoid is then subtracted from the data, leaving a set of residuals, or once-pre-whitened data. The process is repeated with the residual data set, then on the residuals of the twice-pre-whitened data, etc. The sequence is terminated when it is deemed that there are no significant features remaining in the spectrum of the residuals.

The process is illustrated in Fig. 5 for the *V* data – each panel is labelled with the number of frequencies which have been pre-whitened. Inspection of the bottom panel shows that there may

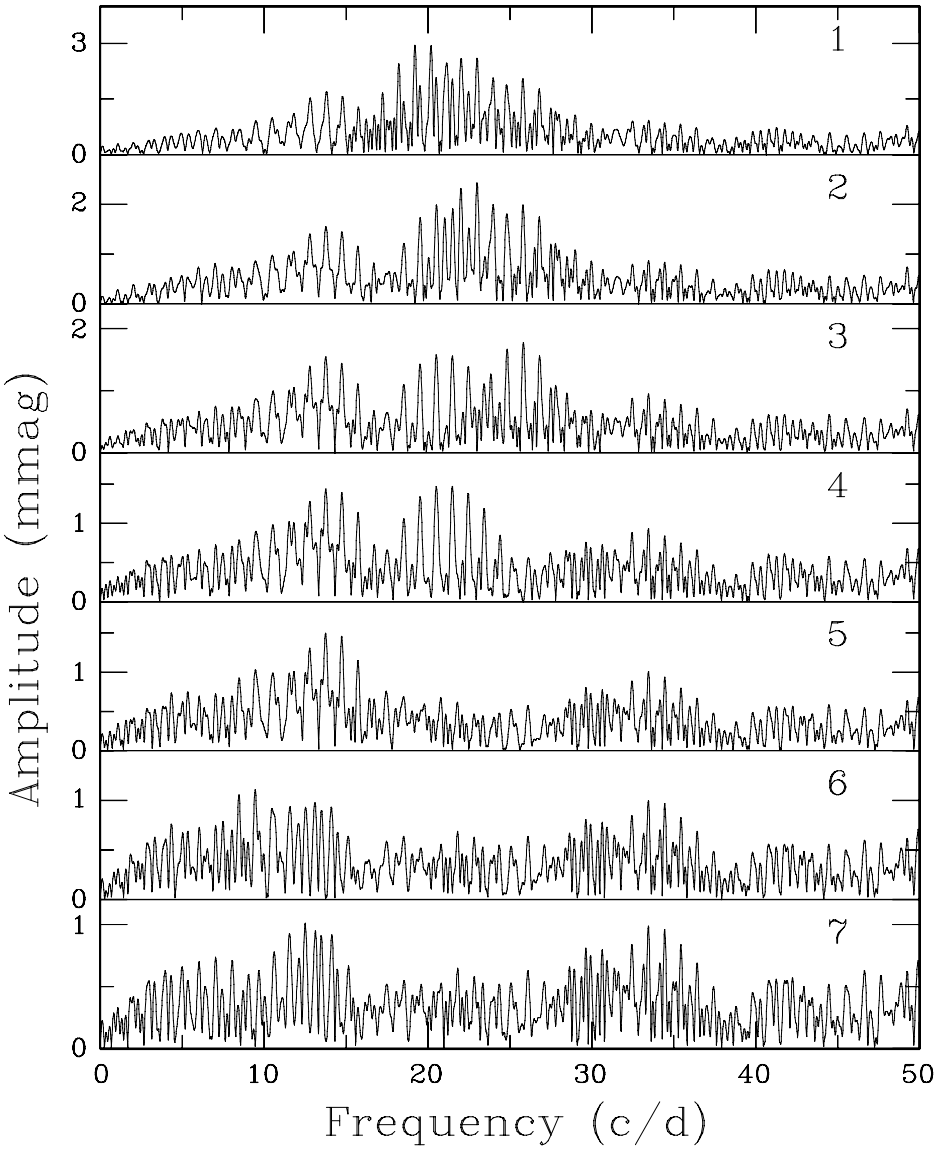

Figure 5. Successive stages of pre-whitening the *V*-band data for PG 0907+123. Each panel is labelled with the number of sinusoids which have been removed from the full data set. Note the different scales on the vertical axes of the different panels.

Table 3. First half: the results of the sequential least-squares fitting and pre-whitening of sinusoids – PG 0907+123 data. Second half: the results of the simultaneous non-linear least-squares fitting of sinusoids to the PG 0907+123 data. The uncertainties in the last quoted digits are given in brackets.

B		*V*		*R*	
Frequency (d^{-1})	Amplitude (mmag)	Frequency (d^{-1})	Amplitude (mmag)	Frequency (d^{-1})	Amplitude (mmag)
14.14(1)	4.7(4)	14.14(1)	4.3(3)	14.15(3)	3.8(5)
19.20(1)	3.5(3)	20.19(1)	3.0(3)	20.34(3)	3.0(4)
22.98(1)	2.9(3)	23.00(2)	2.4(3)	23.11(5)	1.9(4)
24.84(2)	1.8(3)	25.82(2)	1.7(3)	24.79(5)	1.7(3)
21.52(2)	2.0(3)	21.51(2)	1.6(3)		
14.78(2)	1.9(3)	13.77(2)	1.4(3)	14.71(3)	2.7(4)
11.56(2)	1.3(2)	9.46(3)	1.1(2)	9.55(5)	1.8(3)
14.15(1)	3.8(3)	14.14(1)	3.3(3)	14.14(2)	3.6(4)
19.18(1)	3.5(3)	20.18(1)	2.9(3)	20.30(2)	3.2(4)
22.98(2)	2.6(3)	23.01(2)	2.0(3)	23.05(4)	2.0(4)
24.85(2)	2.0(3)	25.82(2)	1.6(3)	24.78(4)	1.9(4)
21.51(2)	2.1(3)	21.50(2)	2.0(3)		
14.77(2)	2.2(3)	13.78(2)	1.6(3)	14.68(2)	3.0(4)
11.60(2)	1.3(3)	9.46(3)	1.1(2)	9.55(4)	1.9(4)

be excesses of power left near 13 and 35 d^{-1}, but there are no convincing corresponding features in the data for the other two filters. The same set of seven frequencies is present in the *B*-band data, although in some cases in the form of 1 d^{-1} aliases. Six of the seven frequencies (or their aliases) could also be identified in the *R*-band data.

The results are listed in the first part of Table 3. The least secure of the frequency correspondences assumed between the different filters is that of $f = 20.34$ in *R*, with $f = 19.20$ and 20.19 d^{-1} in *B* and *V*, respectively. Given the large amplitude of this mode in the *R* band, it is difficult to see any other counterpart amongst the frequencies observed in the other two filters. An alternative is that there is *no* counterpart for $f = 20.34\,d^{-1}$ in *B* and *V*.

The amplitude spectra of the pre-whitened data sets are plotted in Fig. 6. There are no pronounced peaks left, except for the cluster near 18 d^{-1} in the *R*-band data.

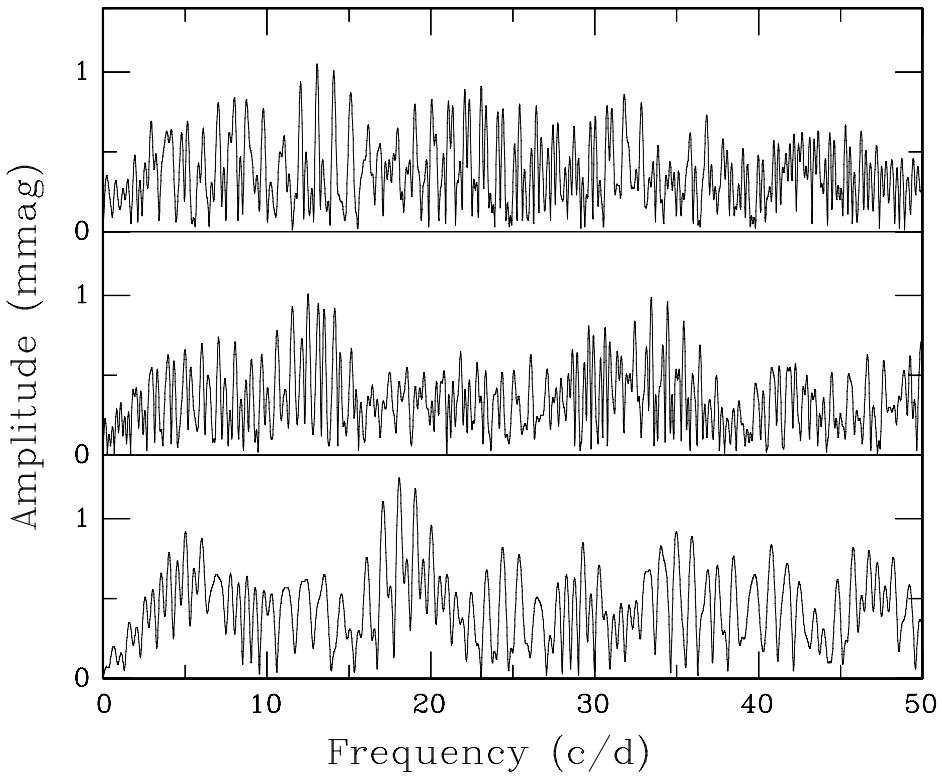

Figure 6. Amplitude spectra of the residuals after pre-whitening the PG 0907+123 *B* and *V* data sequentially by seven sinusoids, and the *R*-band data by six sinusoids. From top to bottom is *B*, *V* and *R*.

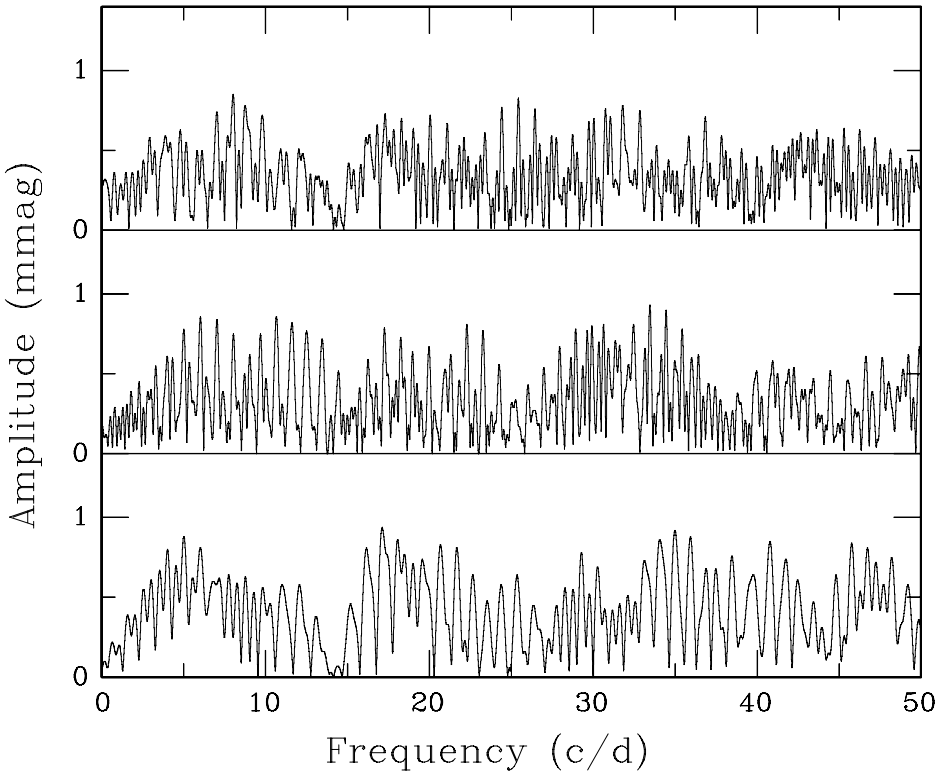

Figure 7. As for Fig. 6, but after pre-whitening by sinusoids simultaneously fitted by a non-linear least-squares method. From top to bottom are *B*, *V* and *R*.

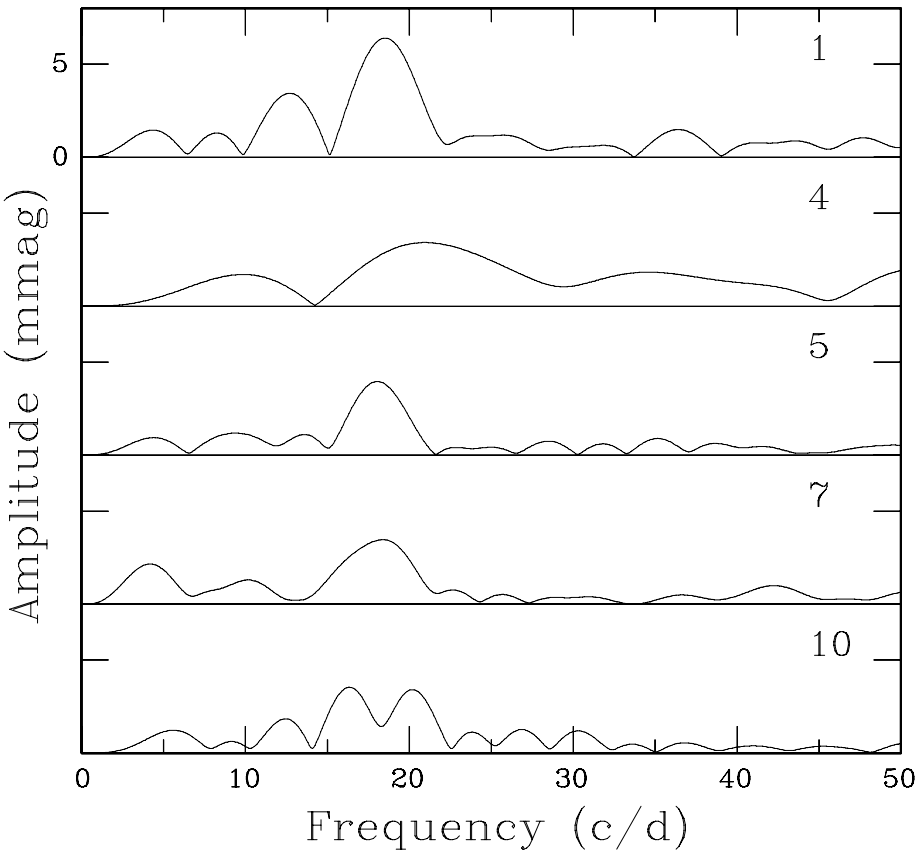

Figure 8. Amplitude spectra of the *V*-band data for JL 194 in Fig. 2. Each night's data were high pass filtered by subtracting a second-order polynomial fit. Panels are labelled with the last digit(s) of the Julian Day of observation.

The figures in the first half of Table 3 (together with the estimated phases) were used as starting values in an iterated simultaneous non-linear least-squares fit of all the sinusoids. The estimated frequencies were virtually identical to those obtained from the sequential linear fitting, but the amplitudes were rather different in some cases (second half of Table 3). Pre-whitening by the fitted sinusoids led to residual spectra with distinctly lower amplitudes than those in Fig. 6 (see Fig. 7).

4 DATA ANALYSIS: JL 194

Fig. 8 contains amplitude spectra of the individual (detrended) JL 194 light curves in Fig. 2. It is tempting to think that the single peaks near 18 d^{-1} in the panels labelled '5' and '7' are resolved into two distinct frequencies in the bottom panel, but the run lengths giving rise to the single peaks are, in fact, slightly longer than that on the last night. Rather, it is the virtually flat light curve

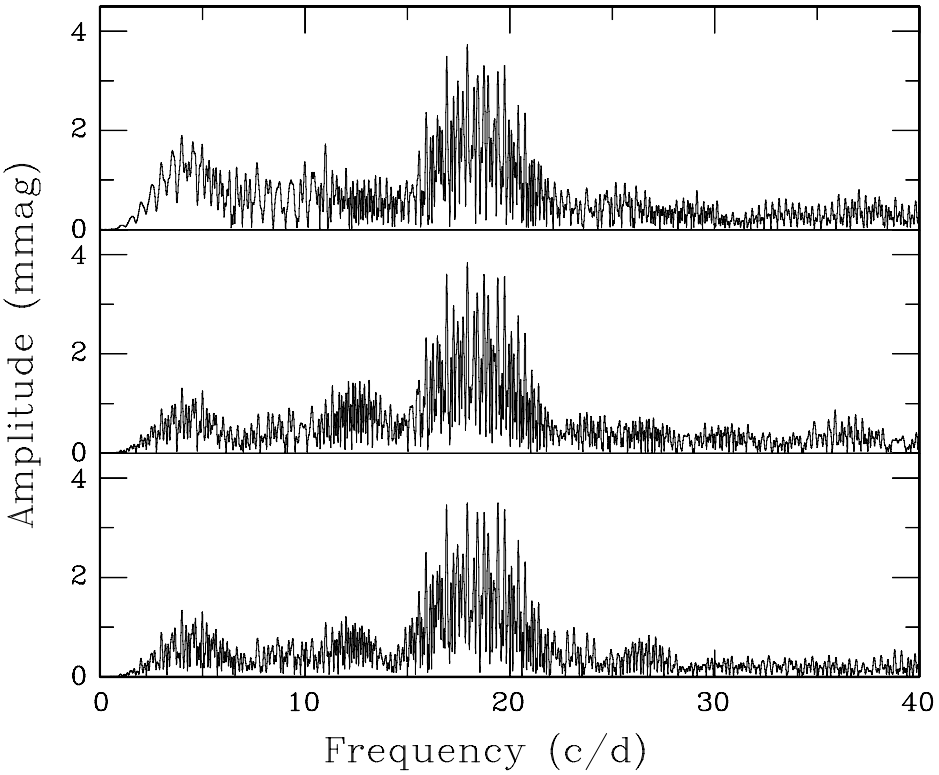

Figure 9. Amplitude spectra of the complete JL 194 data, *B* (top), *V* (middle) and *R* (bottom). Nightly data sets were pre-whitened by subtraction of a least-squares-fitted second-order polynomial.

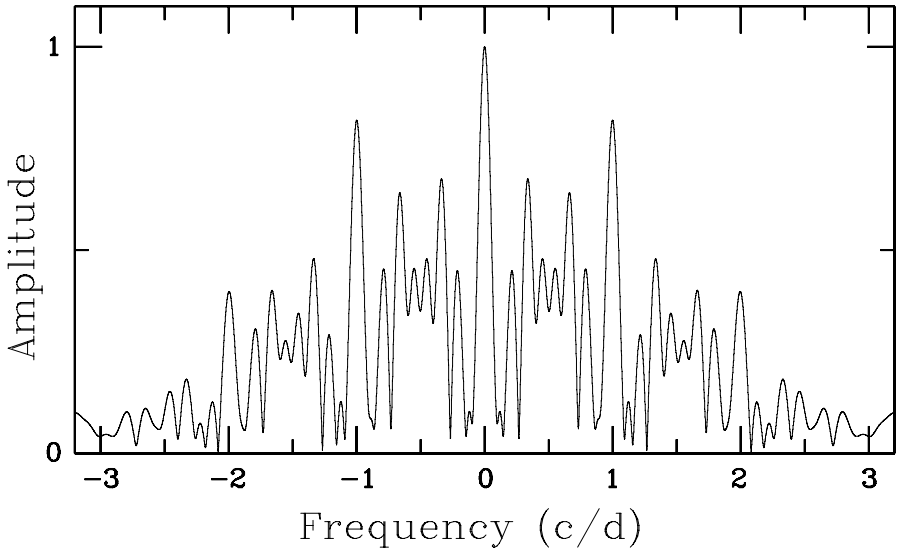

Figure 10. The window function of the JL 194 observations. Note the prominent aliases near 1/3 and 2/3 d^{-1}, in addition to the usual 1 d^{-1} feature.

Table 4. First half: the results of the sequential least-squares fitting and pre-whitening of sinusoids – JL 194 data. Frequencies are presented in the order in which they were extracted from the *B*-band data. Second half: the results of the simultaneous non-linear least-squares fitting of sinusoids to the JL 194 data. The uncertainties in the last quoted digits are given in brackets.

B		*V*		*R*	
Frequency (d^{-1})	Amplitude (mmag)	Frequency (d^{-1})	Amplitude (mmag)	Frequency (d^{-1})	Amplitude (mmag)
17.931(4)	3.7(3)	17.934(4)	3.8(2)	17.929(4)	3.6(2)
19.760(5)	2.7(3)	19.755(4)	2.8(2)	19.761(4)	2.9(2)
17.681(9)	1.5(2)	17.018(9)	1.2(2)	17.000(9)	1.0(2)
11.00(1)	1.4(2)	11.356(8)	1.3(2)	11.02(1)	0.8(2)
21.18(1)	1.4(2)	22.14(1)	0.9(2)	22.152(8)	1.2(2)
17.934(6)	4.2(4)	17.927(3)	4.1(2)	17.915(3)	4.3(2)
19.748(6)	2.7(3)	19.748(4)	2.9(2)	19.758(3)	3.1(2)
18.01(1)	1.8(2)	17.01(1)	1.2(2)		
11.006(8)	1.5(2)	11.353(7)	1.4(2)	11.348(8)	1.1(2)
20.211(8)	1.8(3)	20.209(6)	1.8(2)	19.221(5)	2.3(2)
				22.147(7)	1.2(2)

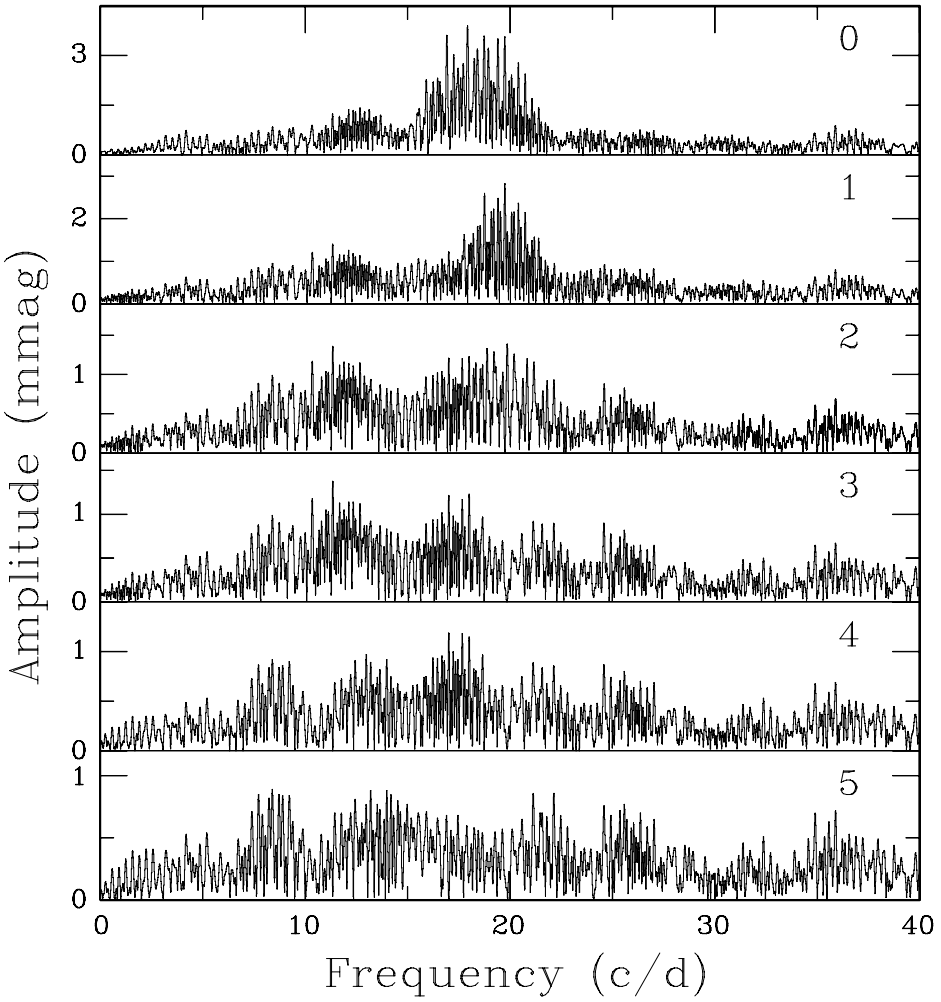

Figure 11. Successive stages of pre-whitening the *V*-band data for JL 194. Each panel is labelled with the number of sinusoids which have been removed from the full data set (excluding the low-frequency removal). Note the different scales on the vertical axes of the different panels.

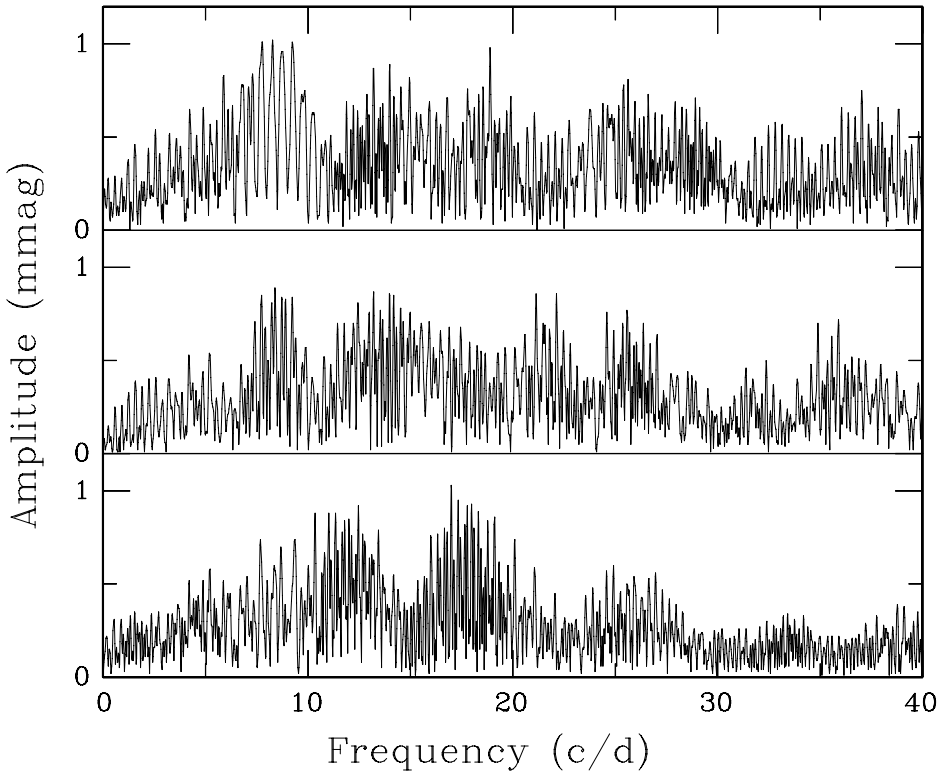

Figure 12. Amplitude spectra of the residuals after pre-whitening each of the three JL 194 data sets by low frequencies (i.e. $f < 5\,\mathrm{d}^{-1}$), and by the five frequencies in the first part of Table 4. From top to bottom are *B*, *V* and *R*.

between JD 245 5090.45 and JD 245 5090.58, bracketed by high amplitude variability, which generates two closely spaced peaks in the amplitude spectrum. Furthermore, given the large changes in the amplitude of the feature near $13\,\mathrm{d}^{-1}$, it is clear that JL 194 has a rich collection of excited modes.

Amplitude spectra of the full data collection are plotted in Fig. 9. Power is primarily concentrated in the frequency range 15–21 d^{-1}, with lesser features around $4\,\mathrm{d}^{-1}$ and, in *V* and *R*, $12\,\mathrm{d}^{-1}$. The complexity of peaks in the dominant interval is impressive, but can, to a large extent, be ascribed to aliasing, induced by the rather sporadic times of observation (Table 2). The window function (Fig. 10) confirms that aliasing is severe: aside from the usual $1\,\mathrm{d}^{-1}$ peak, there are, amongst others, also significant peaks near 1/3 and $2/3\,\mathrm{d}^{-1}$.

As in the case of PG 0907+123, low-frequency power is first pre-whitened from the data. In the case of the *V*- and *R*-band data the best-fitting low frequency is $4.00\,\mathrm{d}^{-1}$; removing this leaves insignificant power below $10\,\mathrm{d}^{-1}$. The low-frequency content of the *B*-band data is more complex, possibly because of the more marked effects of differential extinction: frequencies 3.99, 4.22 and $3.55\,\mathrm{d}^{-1}$ are pre-whitened. It seems likely that all these periodicities are artefacts.

The results of further successive pre-whitening are given in the first part of Table 4, which is the analogue of Table 3, and illustrated in Fig. 11 (the equivalent of Fig. 5). For the first two frequencies the same aliases are selected for each of the three filters; thereafter, 1/3, 2/3 and $1\,\mathrm{d}^{-1}$ aliases are common. None the less, it seems reasonably certain that the same five modes are present in all three data sets.

The amplitude spectra of the three residual data sets (i.e. after removal of the low-frequency features, and the frequencies in the first half of Table 4) are shown in Fig. 12. The *R*-band spectrum seems to bear no relation to the *B* and *V* spectra, which suggests that all the information common to all three filters has been extracted. The reader's attention is also drawn to the excess power near $8\,\mathrm{d}^{-1}$ visible in both the *B*- and *V*-band spectra. It is unclear whether these are artefacts, or due to pulsation modes (see also the discussion of such low-frequency features in Koen 2009).

Simultaneous fitting of five frequencies, by non-linear least squares, gives the results in the second half of Table 4. Comparison with the corresponding entries in the first half of the table shows good agreement for the first two frequencies, across all three filters. The same applies to the $11\,\mathrm{d}^{-1}$ variation – though note that in the case of the *R* band, a different alias is selected. The $17.68\,\mathrm{d}^{-1}$ *B*-band frequency is replaced by a different alias, namely $18.01\,\mathrm{d}^{-1}$ – but remarkably this frequency seems to have disappeared from the *R* band's repertoire. However, a close look at the residual spectrum (bottom panel of Fig. 13) shows that the second-highest peak is at $17.0\,\mathrm{d}^{-1}$. Note also the appearance of $f = 19.22\,\mathrm{d}^{-1}$ in *R*, matching $f = 20.21\,\mathrm{d}^{-1}$ in *B* and *V*.

The residual spectra in Fig. 13 can be compared to those in Fig. 12: note the persistence of the power excesses near $8\,\mathrm{d}^{-1}$ (in *B* and *V*), in both sets of plots.

5 CLOSING REMARKS

The light curve of JL 194 is particularly interesting. The peak-to-peak variation is among the highest seen to date in PG 1716 stars, significantly exceeded only by PG 1627+017 (Randall et al. 2006a) and JL 82 (Koen 2009). It is noteworthy that the temperatures of both these stars are even lower than that of JL 194, and that both are

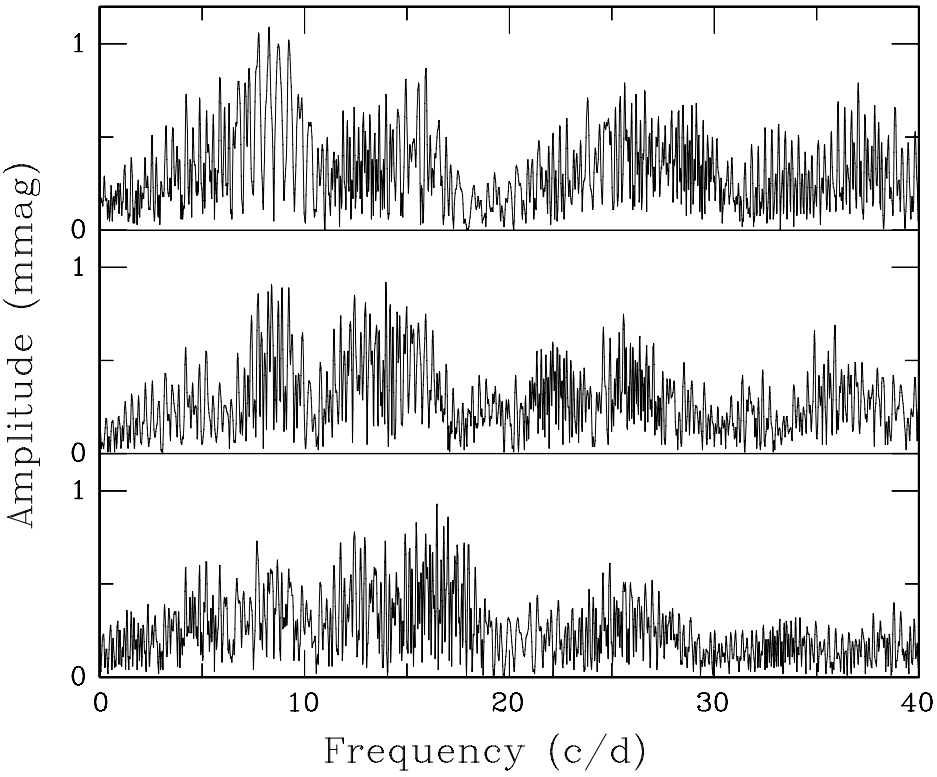

Figure 13. As for Fig. 12, but after pre-whitening by higher frequency sinusoids simultaneously fitted by a non-linear least-squares method (second half of Table 4). From top to bottom are *B*, *V* and *R*.

also low-gravity objects. For PG 1627+017, Morales-Rueda et al. (2003) give $T_{\rm eff} = 21\,600$ K and $\log g = 5.12$, and Randall et al. (2006a) give $T_{\rm eff} = 23\,670$ and $\log g = 5.32$; for JL 82, $T_{\rm eff} = 25\,000$ and $\log g = 5.0$ (Edelmann 2003).

The textbook example of mode interference seen in the bottom panel of Fig. 2 is also very striking. This is due to the concentration of all the modes with significant amplitudes, excluding $f = 11\,{\rm d}^{-1}$, into one narrow frequency interval.

The frequency analyses above should, of course, be seen as indicative only. It is clear that neither the amount nor the time distribution of the observations allows full conclusions to be drawn about the true frequencies of the pulsation modes of the two stars. This

Table 5. A summary of some of the observables of published PG 1716 stars. All frequencies are quoted if three or fewer have been found, otherwise the range of values is given. In the case of the hybrid fast/slowly pulsating stars (Bal 09, HS 0702+6043 and HS 2201+2610) only the lower PG 1716-like frequencies are considered. The *V* magnitudes were taken from Østensen (2006): for HS 0702+6043 and HS 2201+2610 only *B* magnitudes are available, hence *V* was estimated assuming $(B - V) \approx -0.35$.

Star	*V*	No. frequencies	Range (d^{-1})	Max. amplitude (mmag)	Reference
PG 1716+426	14.0	6	15.8–29.4	1.5 (*R*)	1
Balloon 090100001	12.1	4	20.7–31.6 (photometric)	2.6 (*B*)	2
		6	14.6–40.1 (spectroscopic)		2
PG 0101+039	12.1	3	11.9, 16.5, 32.6	0.5 (*MOST*)	3
PG 1627+017	12.9	23	9.7–18.9	4.8 (*R*)	4
PG 1338+481	13.6	13	9.1–40.7	1.9 (*R*)	5
HS 0702+6043	∼13.7	3	17.8, 23.5, 27.5	3.7 (*F555W*)	6
EC 21324−1346	13.2	9	11.1–28.8	3.1 (*B*)	7
KPD 0629−0016	14.9	5	12.3–31.4	3.0 (*B*)	8
HS 2201+2610	∼14.0	1	26.5	1.5 (*B*)	9
JL 82	12.4	>10(?)	5(?)–25(?)	4.5 (*B*)	10
LB 1516	13.0	4	12.2–25.7	2.6 (*B*)	11
PG 0907+123	13.9	7	11.6–24.9	3.8 (*B*)	
JL 194	12.4	5	11.0–20.2	4.2 (*B*)	

References: (1) Reed et al. (2004); (2) Baran, Pigulski & O'Toole (2008); (3) Randall et al. (2005); (4) Randall et al. (2006a); (5) Randall et al. (2006b); (6) Lutz et al. (2008); (7) Kilkenny et al. (2007); (8) Koen & Green (2007); (9) Lutz et al. (2009); (10) Koen (2009); (11) Koen et al. (2010).

aside, it is also clear that both stars have rich pulsation spectra and – at least as far as PG 1716 stars are concerned – large amplitudes. Given that both are also fairly bright, the stars are worthy candidates for multisite campaigns. PG 0907+123 being equatorial is accessible from both hemispheres. The intriguingly high mass derived for the secondary star in the system depends on the assumed mass for the sdB primary, and is yet another good reason for further asteroseismological investigation of this star.

Table 5, which is an updated and expanded version of table 4 in Koen (2009), compares a few properties of all published PG 1716 stars.

ACKNOWLEDGMENTS

The authors are grateful to those maintaining the Simbad data base in Strasbourg, France; to Dr Roy Østensen (Katholieke Universiteit Leuven) for use of his catalogue of hot subdwarf stars (Østensen 2006) and to Professor Gilles Fontaine (Université de Montréal) for communicating to us his unpublished model results for PG 0907+123. CK appreciates allocation of telescope time by SAAO.

REFERENCES

Adelman S. J., 2001, Baltic Astron., 10, 589
Baran A., Pigulski A., Koziel D., Ogloza W., Silvotti R., Zola S., 2005, MNRAS, 360, 737
Baran A., Pigulski A., O'Toole S. J., 2008, MNRAS, 385, 255
Billères M., Fontaine G., Brassard P., Liebert J., 2002, ApJ, 578, 515
Edelmann H., 2003, PhD thesis, Univ. Erlangen-Nürnberg
Fontaine G., Green E. M., Chayer P., Brassard P., Charpinet S., Randall S. K., 2006, Baltic Astron., 15, 211
Green E. M. et al., 2003a, Ap&SS, 284, 65
Green E. M. et al., 2003b, ApJ, 583, L31
Green R. F., Schmidt M., Liebert J., 1986, ApJS, 61, 305
Han Z., Podsiadlowski P., Maxted P. F. L., Marsh T. R., 2003, MNRAS, 341, 669
Heber U., 2009, ARA&A, 47, 211
Heber U., Hunger K., Jonas G., Kudritzki R. P., 1984, A&A, 130, 119
Hill P. W., Hill S. R., 1966, MNRAS, 133, 205
Jaidee S., Lyngrå G., 1969, Arkiv Astron., 5, 345
Jeffery C. S., Pollacco D. L., 1998, MNRAS, 298, 179
Kilkenny D., Hill P. W., 1975, MNRAS, 173, 625
Kilkenny D., Koen C., O'Donoghue D., Stobie R. S., 1997, MNRAS, 285, 640
Kilkenny D., Copley C., Zietsman E., Worters H., 2007, MNRAS, 375, 1325
Koen C., 2009, MNRAS, 395, 979
Koen C., Green E. M., 2007, MNRAS, 377, 1605
Koen C., Kilkenny D., Pretorius M. L., Frew D. J., 2010, MNRAS, 401, 1850
Lutz R. et al., 2008, in Heber U., Jeffery C. S., Napiwotzki R., eds, ASP Conf. Ser. Vol. 392, Hot Subdwarfs and Related Objects. Astron. Soc. Pac., San Francisco, p. 339
Lutz R., Schuh S., Silvotti R., Bernabei S., Dreizler S., Stahn T., Hügelmeyer S. D., 2009, A&A, 496, 469
Maxted P. F. L., Heber U., Marsh T. R., North R. C., 2001, MNRAS, 326, 1391
Moehler S., Richtler T., de Boer K. S., Dettmar R.-J., Heber U., 1990a, A&AS, 86, 53
Moehler S., Heber U., de Boer K. S., 1990b, A&A, 239, 265
Morales-Rueda L., Maxted P. F. L., Marsh T. R., North R. C., Heber U., 2003, MNRAS, 338, 752
Newell B., Graham J. A., 1976, ApJ, 204, 804
Østensen R. H., 2006, Baltic Astron., 15, 85
Østensen R. H., 2009, Communications Asteroseismology, 159, 77
Randall S. K. et al., 2005, ApJ, 633, 460
Randall S. K. et al., 2006a, ApJ, 643, 1198
Randall S. K. et al., 2006b, ApJ, 645, 1464
Reed M. D., Stiening R., 2004, PASP, 116, 506
Reed M. D. et al., 2004, ApJ, 607, 445
Schuh S., Huber J., Dreizler S., Heber U., O'Toole S. J., Green E. M., Fontaine G., 2006, A&A, 445, L31
Skrutskie M. F. et al., 2006, AJ, 131, 1163
Wegner G., 1980, AJ, 85, 538
Wesemael F., Fontaine G., Bergeron P., Lamontagne R., Green R. F., 1992, AJ, 104, 203

This paper has been typeset from a TEX/LATEX file prepared by the author.